Spectral Properties of Prompt Emission of Four Short Gamma-Ray Bursts Observed by the Suzaku-WAM and the Konus-Wind

Masanori Ohno, Yasushi Fukazawa, and Takuya Takahashi

Department of Physical Sciences, School of Science, Hiroshima University,

1-3-1 Kagamiyama, Higashi-Hiroshima, Hiroshima 739-8526

ohno@hirax7.hepl.hiroshima-u.ac.jp

Kazutaka Yamaoka and Satoshi Sugita

Department of Physics and Mathematics, Aoyama Gakuin University, 5-10-1 Fuchinobe, Sagamihara, Kanagawa 229-8558

Valentin Pal'shin, Dmitry Frederiks, Philipp Oleynik, and Mikhail Ulanov

Ioffe Physico-Technical Institute, Laboratory for Experimental Astrophysics,

26 Polytekhnicheskaya, St. Petersburg 194021, Russa

Takanori Sakamoto and Goro Sato

NASA Goddard Space Flight Center, Greenbelt, MD 20771, USA

Kevin Hurley

University of California, Berkeley, Space Sciences Laboratory, 7 Gauss Way, Berkeley, CA 94720-7450, USA

Makoto S. Tashiro, Yuji Urata, and Kaori Onda

Department of Physics, Saitama University, 255 Shimo-Ohkubo, Sakura, Saitama 338-8570

Toru Tamagawa, Yukikatsu Terada, and Motoko Suzuki

Institute of Physical and Chemical Research (RIKEN), 2-1 Hirosawa, Wako, Saitama 351-0198

and

Hong Soojing

Laboratory of Physics College of Science and Technology, Nihon University,

7-24-1 Narashinodai, Funabashi, Chiba 274-8501

Abstract

We have performed a joint analysis of prompt emission from four bright short gamma-ray bursts (GRBs) with the Suzaku-WAM and the Konus-Wind experiments. This joint analysis allows us to investigate the spectral properties of short-duration bursts over a wider energy band with a higher accuracy. We find that these bursts have a high E_{peak}, around 1 MeV and have a harder power-law component than that of long GRBs. However, we can not determine whether these spectra follow the cut-off power-law model or the Band model.

We also investigated the spectral lag, hardness ratio, inferred isotropic radiation energy and existence of a soft emission hump, in order to classify them into short or long GRBs using several criteria, in addition to the burst duration. We find that all criteria, except for the existence of the soft hump, support the fact that our four GRB samples are correctly classified as belonging to the short class. In addition, our broad-band analysis revealed that there is no evidence of GRBs with a very large hardness ratio, as seen in the BATSE short GRB sample, and that the spectral lag of our four short GRBs is consistent with zero, even in the MeV energy band, unlike long GRBs. Although our short GRB samples are still limited, these results suggest that the spectral hardness of short GRBs might not differ significantly from that of long GRBs, and also that the spectral lag at high energies could be a strong criterion for burst classification.

Key words: gamma rays: burst — gamma rays: observations

1. Introduction

The bimodal distribution of the duration of gamma-ray bursts (GRBs) indicates that there are two distinct classes of events. The long-duration bursts have typical durations of around 20 s, while the short-duration bursts (about 1/4 of the total) have durations of around 0.3 s (Mazets et al. 1981; Norris et al. 1984; Dezalay et al. 1992; Hurley 1992; Kouveliotou et al. 1993; Norris et al. 2000). This suggests that the short and long GRBs may have different progenitors. Core collapse of massive stars and mergers of compact binaries are considered likely models for the long and short GRBs, respectively (Katz

& Canel 1996; Ruffert & Janka 1999). Recently, thanks to the rapid position information provided by HETE-2 (Ricker et al. 2003) and Swift (Gehrels et al. 2004), afterglow observations have progressed dramatically and X-ray and optical afterglow emissions were discovered from some short GRBs (Hjorth et al. 2005; Fox et al. 2005), as well as long ones. Some short GRB afterglows have been found to be associated with galaxies not undergoing star formation, while some long GRBs have been found to be associated with energetic supernovae. These results support the hypothesis that long and short GRBs indeed have different progenitors.

From the point of view of prompt gamma-ray emission,

although the spectral characteristics of long GRBs have been well studied (BeppoSAX: Frontera et al. 2000; BATSE: Kaneko et al. 2006; HETE-2: Sakamoto et al. 2005a), our understanding of that of short GRBs is still incomplete, in part due to their very short durations. The spectral characteristics of BATSE short GRBs are often characterized by the hardness ratio, that is, the ratio of 100–300 keV to 25–100 keV counts or fluence (Kouveliotou et al. 1993; Cline et al. 1999). These studies suggest that, although there is considerable overlap, short GRBs tend to be harder than long GRBs. Paciesas et al. (2001) and Ghirlanda, Ghisellini, & Celotti (2004) compared the spectral parameters of bright BATSE short GRBs with those of long GRBs by spectral fitting. They pointed out that the spectra of short GRBs are well described by a cut-off power-law (CPL) model and that the Band model (Band et al. 1993) did not improve the fit. They also confirmed that the spectra of short GRBs are harder than those of long GRBs. This was found to be a consequence of a flat low energy photon index, rather than a difference in the peak energies.

There is another complicating issue in the classification of short and long GRBs. Since their duration distributions overlap, other distinguishing criteria have been proposed, such as differences in the host galaxy (Hjorth et al. 2003, 2005), spectral hardness (Cline et al. 1999), spectral lag (Norris 2002; Norris & Bonnell 2006), isotropic radiation energy (Amati et al. 2002; Amati 2006), and the existence of a soft hump (Norris & Bonnell 2006), or a combination of these and other characteristics (Donaghy et al. 2006). Indeed, some GRBs cannot be classified as short or long using the burst duration alone. For example, GRB 040429 was classified as short using the burst duration (2.39 s), but other properties such as spectral lag and hardness resembled those of long GRBs (Wiersema et al. 2004; Fox & Moon 2004; Donaghy et al. 2006). GRB 051227 (Hullinger et al. 2005; Barthelmy et al. 2005; Sakamoto et al. 2005b) had a long enough duration of 8.0 s to be classified as long. However, this burst had no significant spectral lag in the initial spike, which is seen in many long GRBs (Norris et al. 1996), and it also had a long soft hump in the light curve. These two properties are similar to those of short GRBs. GRB 060614 (Gehrels et al. 2006) exhibited a long duration (102 s). However, it did not have any significant spectral lag in the initial spike, and also there were no signs of any associated supernova, despite its distance of $z = 0.125$, which should have been close enough to detect it. These examples show why the burst duration should no longer be considered a sole indicator for distinguishing between the short and long classes of bursts. Indeed Donaghy et al. (2006) have suggested the terms "short population bursts" and "long population bursts" to distinguish the two classes. In this paper, we will use simply "short" and "long" to describe these classes.

Here, we report on the joint spectral analysis of four bright short GRBs simultaneously observed by the Suzaku-WAM (Suzaku Wide-band All-sky Monitor) and Konus-Wind. The WAM and Konus have wide energy ranges, from 50–5000 keV and 10–10000 keV, respectively, and the WAM has the largest effective area from 300 keV to 5000 keV of any current experiment with spectral capabilities. Thus, we can investigate the spectral characteristics of short GRBs up to MeV energies. We also classify the four GRBs as short or long using our data with

high statistics up to the MeV energy region using a number of criteria: spectral lag, hardness ratio, isotropic radiation energy, and existence of a soft hump.

2. Instruments and Observations

2.1. Instruments

2.1.1. Suzaku-WAM

The Suzaku Wide-band All-sky Monitor (WAM) is the active shield of the Hard X-ray Detector (HXD) (Takahashi et al. 2007; Kokubun et al. 2007) aboard Suzaku (Mitsuda et al. 2007). It consists of large-area, thick BGO crystals, and is also designed to monitor the entire sky from 50 keV to 5 MeV with a large effective area. The large effective area from 300 keV to 5 MeV (400 cm^2 even at MeV) surpasses those of other currently operating experiments with spectral capability, and enables us to perform wide-band spectroscopy of GRBs with high sensitivity (Yamaoka et al. 2005, 2006). The WAM is subdivided into four detectors, numbered WAM 0 to WAM 3, located at each side of the main detector of the HXD. We utilize the azimuthal [ϕ (degree)] and zenith [θ (degree)] angle to determine the incident direction of GRBs. The azimuthal zero angle ($\phi = 0$) is defined to be perpendicular to the WAM 1 detector plane, and it increases in the order WAM 0, WAM 3, and WAM 2. The WAM 0 detector faces the solar paddle of the satellite and it always views the solar direction. The polar axis that defines the zenith angle θ is toward the Suzaku field-of-view of the main detectors. Thus the on-axis direction of each WAM detector corresponds to (θ, ϕ) = (90, 0) for WAM 1, (90, 90) for WAM 0, (90, 180) for WAM 3, and (90, 270) for WAM 2.

The WAM outputs two data types, the transient (TRN) data and the gamma-ray burst (GRB) data. The TRN data are always accumulated with 1 s time resolution and 55 energy channels. This can be used to monitor the bright soft gamma-ray sources with the Earth occultation method, as was done by CGRO/BATSE (Ling et al. 2000). On the other hand, the GRB data are recorded only for 64 s when the GRB trigger is activated, and the data cover 8 s before and 56 s after the trigger time. The GRB data have four energy channels with 1/64 s time resolution, in addition to the spectral data in 55 pulse height channels with 0.5 s time resolution. This allows us to perform both spectroscopy and timing analysis using the GRB data. In the initial phase before 2006 March 20, these two time resolutions for GRB data were set to 1/32 s and 1.0 s, respectively.

The response matrix of the WAM is very complicated, depending on both the azimuthal and zenith angles of GRBs, because the WAM is inside the satellite body and suffers heavy absorption from it. In order to calculate the detector response of the WAM, we utilize a Monte Carlo simulation based on the Geant4 code, including many kinds of detector characteristics. In the pre-flight calibration, we measured these detector characteristics and developed a WAM response generator (Ohno et al. 2005). From the results of this pre-flight calibration, we found that the response generator can reproduce the measured spectral shape, but the measured effective area of the WAM varies drastically, depending on the gamma-ray incident angle. The trend of this angular response is different among the four WAM detectors. The angular responses of the WAM 1 and

Table 1. Interplanetary network spacecraft observations of the four WAM and Konus short GRBs.

Trigger time (UT)		Spacecraft[*,†]
Suzaku-WAM	Konus-Wind	
GRB 051127		
22:55:19.896	22:55:15.860	Konus, Suzaku, Odyssey HEND, HETE-FREGATE
GRB 060317		
11:17:39.104	11:17:35.996	Konus, Suzaku, INTEGRAL SPI-ACS
GRB 060429		
12:19:51.031	12:19:49.712	Konus, Suzaku, Odyssey HEND & GRS, INTEGRAL SPI-ACS, RHESSI
GRB 060610		
11:22:23.544	11:22:22.632	Konus, Suzaku, Odyssey HEND & GRS, INTEGRAL SPI-ACS, RHESSI

[*] HEND and GRS are the High Energy Neutron Detector and Gamma-ray Sensor head (Hurley et al. 2006a)
[†] SPI-ACS is the spectrometer anti-coincidence detector (Rau et al. 2005)

WAM 3 detectors are complicated, and this trend is similar in both cases. We believe that this is caused by absorption from numerous electronics devices attached inside the satellite panels. The WAM 2 detector is the most heavily affected, since the Ne/He chamber for the X-Ray Spectrometer (XRS) is located inside the WAM 2 field-of-view. This is not the case for the angular response of the WAM 0 detector, and it can be approximately described by a simple cosine function. This is because only the solar paddle is attached to the satellite panel, facing the WAM 0 detector.

In order to estimate the uncertainty in the angular response, we performed an in-flight cross-calibration between the WAM, Konus, and the Swift/BAT, using the data of simultaneously detected GRBs, and found that the measured spectral shapes agree quite good up to the MeV energy region, but that the observed flux fluctuates typically by 10–20% and by 40% at most above 100 keV. This uncertainty is consistent with pre-launch expectations. Below 100 keV, there are still larger flux uncertainties of about 50%. We also confirmed that the WAM 0 detector has the most reliable detector response, with a flux uncertainty of 20% (T. Sakamoto et al. 2008, in preparation).

2.1.2. Konus-Wind

The Konus-Wind instrument (Aptekar et al. 1995) is a gamma-ray spectrometer aboard the GGS-Wind spacecraft. It consists of two identical detectors, S1 and S2, which observe correspondingly the south and north ecliptic hemispheres in an all-sky monitoring mode. Each detector is a cylindrical NaI(Tl) crystal 13 cm in diameter and 7.5 cm in height. The experiment operates in triggered and waiting modes. In the triggered mode the burst time histories are recorded in three energy windows (G1, G2, and G3) 0.512 s before and 229.632 s after the trigger, with a variable time resolution from 2 ms up to 256 ms. 64 energy spectra are measured in two partially overlapping energy ranges, nominally 10–750 keV and 0.2–10 MeV. In each range they are recorded in 63 channels with time resolutions starting at 64 ms, and subsequent spectra have resolutions from 256 ms to 8.192 s. In the waiting mode, each detector measures the count rate with a resolution of 2.944 s in three energy windows. For the GRBs considered here, the actual spectral ranges were 21 keV–16 MeV for the S1 detector and 18 keV–

14 MeV for the S2 detector; the actual time history windows were 21–83, 83–360, 360–1360 keV (S1), and 18–70, 70–300, 300–1160 keV (S2). The detector response matrices depend only on the zenith (θ) angle because of its axi-symmetric structure.

2.1.3. The Interplanetary Network

The Interplanetary Network (IPN) is a group of spacecrafts with gamma-ray burst detectors. Its main purpose is to monitor the entire sky for gamma-ray bursts with close to a 100% duty cycle, and to localize bursts with up to arcminute accuracy. This is done by comparing the arrival times of a GRB among the spacecrafts. Since the third IPN began operations in 1990, over 25 spacecrafts have participated in it, including Konus-Wind (Hurley et al. 2006a). The Suzaku-WAM is the latest experiment to join the IPN. It now plays an important role in it, and many GRBs have already been localized using WAM data (Golenetskii et al. 2006a; Cummings et al. 2006; Hurley et al. 2006b; Golenetskii et al. 2006b).

When a burst is detected by three widely separated spacecrafts, a very accurate localization can usually be obtained. For the bursts discussed here, however, the Ulysses GRB experiment was off, and Mars Odyssey was the only interplanetary spacecraft. The resulting error boxes in this case tend to be large. Table 1 shows which spacecraft observed the events discussed in this paper. Note that GRB 060317 was not observed by Mars Odyssey, and therefore the uncertainty in its localization is the largest. Table 2 gives the final coordinates of the error boxes. In most cases, the error boxes were not small enough and/or determined rapidly enough to warrant follow-up searches. In the case of GRB 060429, however, GCN Circulars were issued (Hurley et al. 2006b; Golenetskii et al. 2006b), and a Swift target of opportunity observation was carried out. However, for this and the other events, no counterparts were identified at any wavelength.

2.2. The Short GRB Sample

More than 70 GRBs triggered the WAM and Konus simultaneously between 2005 August to 2006 October. In order to perform joint spectral analysis of short GRBs, we selected well localized short GRBs and constructed detector response

Table 2. Error box centers and corners of IPN localization and incident angle.

GRB	Area sq. deg.	$\alpha_{2000.0}$	$\delta_{2000.0}$		Incident angle (°)*	
					θ, ϕ (WAM)	θ (Konus)
051127	0.13	301.500	−37.782	(center)	56.3, 80.2	17.4
		301.371	−36.873		56.6, 79.1	
		301.695	−38.523		56.4, 78.6	
		301.622	−38.663		56.0, 81.2	
		301.302	−37.024		56.6, 79.3	
060317	5.3	301.900	−10.882	(center)	125.0, 49.5	9.1
		301.391	−17.546		131.7, 49.5	
		301.976	−8.163		122.3, 49.4	
		303.343	−4.329		118.4, 50.7	
		301.987	−13.575		127.7, 49.9	
060429	0.14	115.314	−24.926	(center)	146.1, 134.1	45.5
		115.307	−24.932		146.1, 134.1	
		113.108	−25.520		145.5, 130.5	
		117.509	−24.233		146.5, 137.8	
		115.321	−24.919		146.0, 134.0	
060610	0.013	354.762	52.107	(center)	41.1, 23.6	48.3
		354.294	52.375		40.7, 23.5	
		354.260	52.417		40.6, 23.5	
		355.227	51.835		41.4, 23.7	
		355.261	51.793		41.5, 23.7	

* θ and ϕ are the zenith and azimuthal angles, respectively, in degrees.

matrices. Only 8 short GRBs were localized well enough by Swift and/or the IPN in this period, and 4 of them (GRB 051127, GRB 060317, GRB 060429, and GRB 060610) had hard enough spectra to detect in the highest energy band light curves of both instruments. Therefore, we selected them to investigate the spectral properties of short GRBs up to the MeV energy region.

GRB 051127 triggered the WAM and Konus at T_0(WAM) = 22:55:19.896 UT and T_0(KW) = 22:55:15.860 UT, 2005 November 27. The incidence angles on the detectors could be determined thanks to the IPN localization (K. Hurley 2005, private communication). The incident direction of this GRB was the nearest to on-axis for the WAM 0 detector of the four, and thus the uncertainty in the detector response is the lowest for the WAM. GRB 060317 was very bright and it triggered the WAM and Konus at T_0(WAM) = 11:17:39.104 UT and T_0(KW) = 11:17:35.996 UT, 2006 March 17. The incidence angle on the WAM was also good for the WAM 0 detector. At T_0(WAM) = 12:19:51.031 UT and T_0(KW) = 12:19:49.712 UT, 2006 April 29, the WAM and Konus detected the bright short GRB 060429. GRB 060610 triggered the WAM 1 detector and the S2 detector of Konus at T_0(WAM) = 11:22:23.544 UT and T_0(KW) = 11:22:22.632 UT, 2006 June 10. For this GRB, the incident direction was closer to on-axis for the WAM 1 detector than WAM 0. However, this angle was determined to be good in the cross-calibration, and the flux uncertainty still should be within 20%. The detections are summarized in table 2.

3. Data Analysis

We performed spectral analysis by applying three spectral models. The first one is a simple power-law (PL) model,

$$N(E) = A \times (E/100)^{\alpha}, \tag{1}$$

where A is the normalization constant at $100\,\mathrm{keV}$ in photons $\mathrm{cm}^{-2}\,\mathrm{s}^{-1}\,\mathrm{keV}^{-1}$, and α is the power-law photon index.

The second model is a power-law with an exponential cutoff (CPL) model,

$$N(E) = A \times \left(\frac{E}{100}\right)^{\alpha} \exp\left[-\frac{E(2+\alpha)}{E_{\mathrm{peak}}}\right], \tag{2}$$

where E_{peak} is the peak energy in the νF_ν spectrum, and represents the energy at which most of the power is emitted.

The third model is a smoothly connected broken power-law model known as the Band model (Band et al. 1993):

$$
\begin{aligned}
N(E) = {} & A \times \left(\frac{E}{100}\right)^{\alpha} \exp\left[-\frac{E(2+\alpha)}{E_{\mathrm{peak}}}\right], \\
& \quad \text{for } E < \frac{(\alpha-\beta)E_{\mathrm{peak}}}{(2+\alpha)} \\
& A \times \left(\frac{E}{100}\right)^{\beta} \left[\frac{(\alpha-\beta)E_{\mathrm{peak}}}{100(2+\alpha)}\right]^{(\alpha-\beta)} \exp(\beta-\alpha), \\
& \quad \text{for } E \geq \frac{(\alpha-\beta)E_{\mathrm{peak}}}{(2+\alpha)}, \tag{3}
\end{aligned}
$$

where α is the power-law photon index in the lower energy band, and β is the index in the higher energy band.

First, we performed fits for each instrument alone. After confirming the consistency between the WAM and Konus, we performed a joint fit. Selecting the time regions was important for this analysis because the WAM and Konus have different time resolutions for the spectral data. As mentioned in section 2, the WAM has a 1.0 or 0.5 s time resolution for spectral data, and can accumulate spectra both before and after the GRB trigger. On the other hand, Konus can accumulate spectra only after the trigger, and the time resolution varies depending on the burst intensity. In the case of the four short GRBs analyzed here, the time resolution of the Konus spectra is 64 ms for first four intervals and 8.192 s for remainder. Therefore, the time regions cannot be completely identical for the WAM and Konus, and we have selected the times for each instrument that are as close as possible between the two. To account for the differences in the accumulation times, we introduced a constant factor in the joint fits. The background spectra were extracted from both before and after the WAM time regions, but only after the time region for Konus. As mentioned in subsubsection 2.1.1, the detector response of the WAM strongly depends on the position of the GRB, and thus the error box of the IPN localization might cause some uncertainties for spectral analysis of the WAM. In order to estimate this effect, we calculated the detector response of the WAM for all corners of the box, as shown in table 2, and performed spectral analysis by using each of them. This uncertainty is included as the systematic error. We used XSPEC version 11.3.2 for spectral analysis (Arnaud 1996). Throughout this paper, the quoted uncertainties are given at the 90% confidence level for one interesting parameter. A summary of the fitting results is given in table 3 and table 4.

We also examined the spectral lag using the cross-correlation function (CCF) between the light curves in two energy bands (Norris 2002; Norris & Bonnell 2006; Link et al. 1993; Band 1997; Yi et al. 2006). If $v_1(t)$ and $v_2(t)$ are the light curves in two different energy bands, the CCF is defined by

$$\mathrm{CCF}(\tau_{\mathrm{lag}}) = \frac{\sum_t v_1(t) v_2(t + \tau_{\mathrm{lag}})}{N \sqrt{\sigma_{v_1} \sigma_{v_2}}},$$

$$\text{where} \quad \sigma_v^2 = \frac{1}{N} \sum_{i=1}^{N} v_i^2, \tag{4}$$

where N is the number of data points in the light curve. We used four energy bands for WAM light curves: 50–110 keV, 110–240 keV, 240–520 keV, and 520–5000 keV. After calculating the CCF as a function of lag τ_{lag}, we obtained the peak value of τ_{lag} by fitting it with a Gaussian profile (Yi et al. 2006). In this formula, positive spectral lag means that the spectrum has hard to soft evolution.

3.1. GRB 051127

The WAM and Konus light curves of GRB 051127 are shown in figure 1. The WAM light curve contains multiple spikes, and the T_{90} duration (the time to accumulate between 5 and 95% of the counts), which is measured between 50 and 5000 keV, is 0.66 s. Thus, this burst is classified as short, using the burst duration alone. We extracted the spectrum from $T_0(\mathrm{WAM})$ to $T_0(\mathrm{WAM}) + 1.0$ s for the WAM and $T_0(\mathrm{KW})$ to $T_0(\mathrm{KW}) + 0.256$ s for Konus, where the trigger times of the

WAM and Konus, $T_0(\mathrm{WAM})$ and $T_0(\mathrm{KW})$, are summarized in table 1 and shown in figure 1. The propagation delay from Suzaku to Wind is 4.364 s for this GRB, i.e., correcting for this factor, one sees that the $T_0(\mathrm{KW}) = T_0(\mathrm{WAM}) + 0.328$ s. We cannot adjust the time region further because the next Konus time bin has a duration of 8.192 s. The emission is clearly seen up to 5 MeV for the WAM and up to 2 MeV for Konus, as shown in figure 2. We thus performed a fit from 100 keV to 5 MeV for the WAM and from 20 keV to 2 MeV for Konus. The WAM spectrum is well described by the CPL model with a photon index of $-0.50^{+0.18}_{-0.18}$ and a peak energy E_{peak} of 1257^{+280}_{-192} keV. For Konus, the same model with a photon index of $-0.29^{+0.29}_{-0.21}$ and an E_{peak} of 940^{+280}_{-180} keV provides the best fit. The WAM spectrum seems to be slightly softer than that of Konus. We believe that this is because it includes a soft emission peak around $T = T_0(\mathrm{WAM}) - 0.2$ s. There are no significant differences in χ^2 between the CPL and the Band model fits for either spectrum. The power-law photon index, α, in the low-energy portion and the peak energy, E_{peak}, are consistent with those obtained by the CPL model. However, we cannot constrain the power-law photon index, β, at high energies and obtain only an upper limit of $\beta < -2.03$. We then performed a joint fit. The CPL model with a photon index $-0.44^{+0.15}_{-0.15}$ and E_{peak} 1168^{+207}_{-150} keV provides the best fit. Table 3 summarizes the results of all of the conducted fits.

3.2. GRB 060317

There are two intense pulses in the light curve of GRB 060317, as seen in figure 1. The burst has a total duration of about 1.31 s for the WAM. We cannot distinguish whether this GRB belongs to the short or long population from the burst duration alone, because the duration distribution overlaps around 1–2 s. In order to extract the spectrum from both pulses, the WAM time region was taken to be $T_0(\mathrm{WAM})$ to $T_0(\mathrm{WAM}) + 4.0$ s. For Konus, we had to select a larger time region than that of the WAM, so as to include both pulses: from $T_0(\mathrm{KW})$ to $T_0(\mathrm{KW}) + 8.336$ s. Konus detected this burst 3.497 s before detection by the WAM, and thus $T_0(\mathrm{KW})$ corresponds to $T_0(\mathrm{WAM}) + 0.389$ s. We can see that emission is clearly detected up to 5 MeV for the WAM and up to 10 MeV for Konus, as shown in figure 2. Therefore, we performed the spectral fitting from 100 keV to 5 MeV for the WAM and from 20 keV to 10 MeV for Konus. We cannot constrain E_{peak} from the WAM spectrum, and a simple power-law with a photon index of $-1.11^{+0.05}_{-0.05}$ fits the observed spectrum well. On the other hand, the Konus spectrum is well described by the CPL model with a photon index of $-1.02^{+0.15}_{-0.13}$ and an E_{peak} of 2089^{+1199}_{-634} keV. The Band model does not provide any improvement to the fit. When we performed the joint fit, E_{peak} became very large (5687^{+3032}_{-1672} keV). This might come from the large IPN error box, which is about 5 deg^2, and the systematic uncertainty might be larger than our estimation. Therefore, we take the spectral parameters of this burst to be those obtained by Konus.

3.3. GRB 060429

This GRB shows a very simple short spike structure with a duration of 0.08 s in the WAM light curve (figure 1); based

Table 3. Results of spectral fittings.

Model	Detector	α^*	$\beta^\dagger$	E_{peak} [keV]	Norm[‡]	Const[§]	χ^2/d.o.f.
				GRB 051127			
PL	WAM 0	$-1.24^{+0.05}_{-0.05}$	—	—	$3.78^{+0.41}_{-0.36}$	—	142/24
	KW(S1)	$-1.07^{+0.07}_{-0.07}$	—	—	$4.67^{+0.58}_{-0.59}$	—	70/31
	WAM 0+KW(S1)	$-1.22^{+0.05}_{-0.04}$	—	—	$5.30^{+0.48}_{-0.54}$	$0.67^{+0.10}_{-0.07}$	229/56
CPL	WAM 0	$-0.50^{+0.18}_{-0.18}$	—	1257^{+280}_{-192}	$2.58^{+0.40}_{-0.35}$	—	29/23
	KW(S1)	$-0.29^{+0.29}_{-0.21}$	—	940^{+280}_{-181}	$5.37^{+0.87}_{-0.82}$	—	32/30
	WAM 0+KW(S1)	$-0.44^{+0.15}_{-0.15}$	—	1168^{+207}_{-150}	$5.18^{+0.57}_{-0.57}$	$0.50^{+0.07}_{-0.06}$	64/55
Band	WAM 0	$-0.30^{+0.18}_{-0.24}$	< -2.08	999^{+347}_{-273}	$2.48^{+0.40}_{-0.31}$	—	32/22
	KW(S1)	$-0.34^{+0.19}_{-0.17}$	< -2.03	$999^{+58.5}_{-187}$	$5.30^{+0.87}_{-0.83}$	—	32/29
	WAM 0+KW(S1)	$-0.32^{+0.13}_{-0.10}$	< -2.33	1038^{+185}_{-110}	$5.16^{+0.58}_{-0.56}$	$0.48^{+0.06}_{-0.06}$	64/54
				GRB 060317			
PL	WAM 0	$-1.11^{+0.05}_{-0.06}$	—	—	$2.14^{+0.48}_{-0.34}$	—	54/25
	KW(S2)	$-1.32^{+0.05}_{-0.05}$	—	—	$0.90^{+0.08}_{-0.08}$	—	74/50
	WAM 0+KW(S2)	$-1.16^{+0.05}_{-0.05}$	—	—	$0.70^{+0.08}_{-0.08}$	$3.27^{+0.25}_{-0.24}$	167/76
CPL	WAM 0	$-1.03^{+0.05}_{-0.06}$	—	>5000	$2.06^{+0.48}_{-0.33}$	—	50/24
	KW(S2)	$-1.02^{+0.15}_{-0.13}$	—	2089^{+1200}_{-634}	$0.87^{+0.09}_{-0.09}$	—	53/49
	WAM 0+KW(S2)	$-1.03^{+0.08}_{-0.09}$	—	5687^{+3092}_{-1672}	$0.70^{+0.08}_{-0.08}$	$3.07^{+0.25}_{-0.22}$	144/75
Band	WAM 0	$-0.99^{+0.11}_{-0.14}$	$-2.50^{+0.06}_{-0.09}$	>5000	$2.02^{+0.48}_{-0.33}$	—	47/23
	KW(S2)	$-0.85^{+0.34}_{-0.06}$	< -2.73	997^{+1089}_{-1281}	$0.93^{+0.08}_{-0.10}$	—	55/48
	WAM 0+KW(S2)	$-0.99^{+0.04}_{-0.15}$	< -1.58	3230^{+6743}_{-2232}	$0.76^{+0.03}_{-0.14}$	$2.74^{+0.26}_{-0.19}$	128/74
				GRB 060429			
PL	WAM 0	$-1.24^{+0.12}_{-0.10}$	—	—	$3.66^{+1.15}_{-0.78}$	—	42/25
	KW(S1)	$-1.27^{+0.04}_{-0.04}$	—	—	$9.55^{+0.85}_{-0.85}$	—	98/33
	WAM 0+KW(S1)	$-1.26^{+0.05}_{-0.04}$	—	—	$9.50^{+0.88}_{-0.85}$	$0.40^{+0.05}_{-0.05}$	140/59
CPL	WAM 0	$-0.99^{+0.26}_{-0.28}$	—	>1430	$3.29^{+1.21}_{-0.83}$	—	37/24
	KW(S1)	$-0.76^{+0.15}_{-0.13}$	—	1583^{+492}_{-371}	$11.0^{+1.17}_{-1.14}$	—	30/32
	WAM 0+KW(S1)	$-0.80^{+0.12}_{-0.13}$	—	1720^{+504}_{-384}	$10.9^{+1.13}_{-1.06}$	$0.28^{+0.07}_{-0.05}$	70/58
Band	WAM 0	$-0.99^{+0.55}_{-0.21}$	< -1.28	>1000	$3.29^{+0.78}_{-0.85}$	—	37/23
	KW(S1)	$-0.62^{+0.14}_{-0.29}$	< -2.02	1560^{+499}_{-656}	$11.0^{+1.25}_{-1.09}$	—	30/31
	WAM 0+KW(S1)	$-0.62^{+0.12}_{-0.17}$	< -1.67	1251^{+519}_{-581}	$11.2^{+0.97}_{-1.10}$	$0.27^{+0.07}_{-0.05}$	73/57
				GRB 060610			
PL	WAM 1	$-1.16^{+0.08}_{-0.09}$	—	—	$3.46^{+0.82}_{-0.73}$	—	38/25
	KW(S2)	$-1.33^{+0.04}_{-0.04}$	—	—	$6.25^{+0.48}_{-0.48}$	—	123/50
	WAM 1+KW(S2)	$-1.29^{+0.04}_{-0.05}$	—	—	$5.98^{+0.52}_{-0.53}$	$0.66^{+0.14}_{-0.12}$	175/76
CPL	WAM 1	$-0.90^{+0.17}_{-0.22}$	—	2889^{+2973}_{-1175}	$3.11^{+0.83}_{-0.74}$	—	24/24
	KW(S2)	$-0.94^{+0.12}_{-0.11}$	—	1536^{+500}_{-366}	$7.18^{+0.66}_{-0.63}$	—	67/49
	WAM 1+KW(S2)	$-0.92^{+0.09}_{-0.12}$	—	1821^{+495}_{-364}	$6.71^{+0.63}_{-0.67}$	$0.52^{+0.11}_{-0.09}$	104/75
Band	WAM 1	$-0.81^{+0.18}_{-0.23}$	< -8.82	1799^{+1855}_{-817}	$3.12^{+0.83}_{-0.73}$	—	24/23
	KW(S2)	$-0.99^{+0.15}_{-0.04}$	< -2.21	1531^{+528}_{-414}	$7.29^{+0.58}_{-0.73}$	—	69/48
	WAM 1+KW(S2)	$-0.88^{+0.10}_{-0.13}$	< -2.50	1687^{+634}_{-688}	$6.70^{+0.65}_{-0.71}$	$0.50^{+0.16}_{-0.07}$	102/74

[*] Power law photon index for the PL and CPL model, and low energy index for the Band model.
[†] Power law photon index for the high energy component of the Band model.
[‡] Normalization in photons $\mathrm{keV^{-1}\,cm^{-2}\,s^{-1}}$ at 100 keV.
[§] Constant factor for the WAM to Konus normalization in joint spectral fittings.
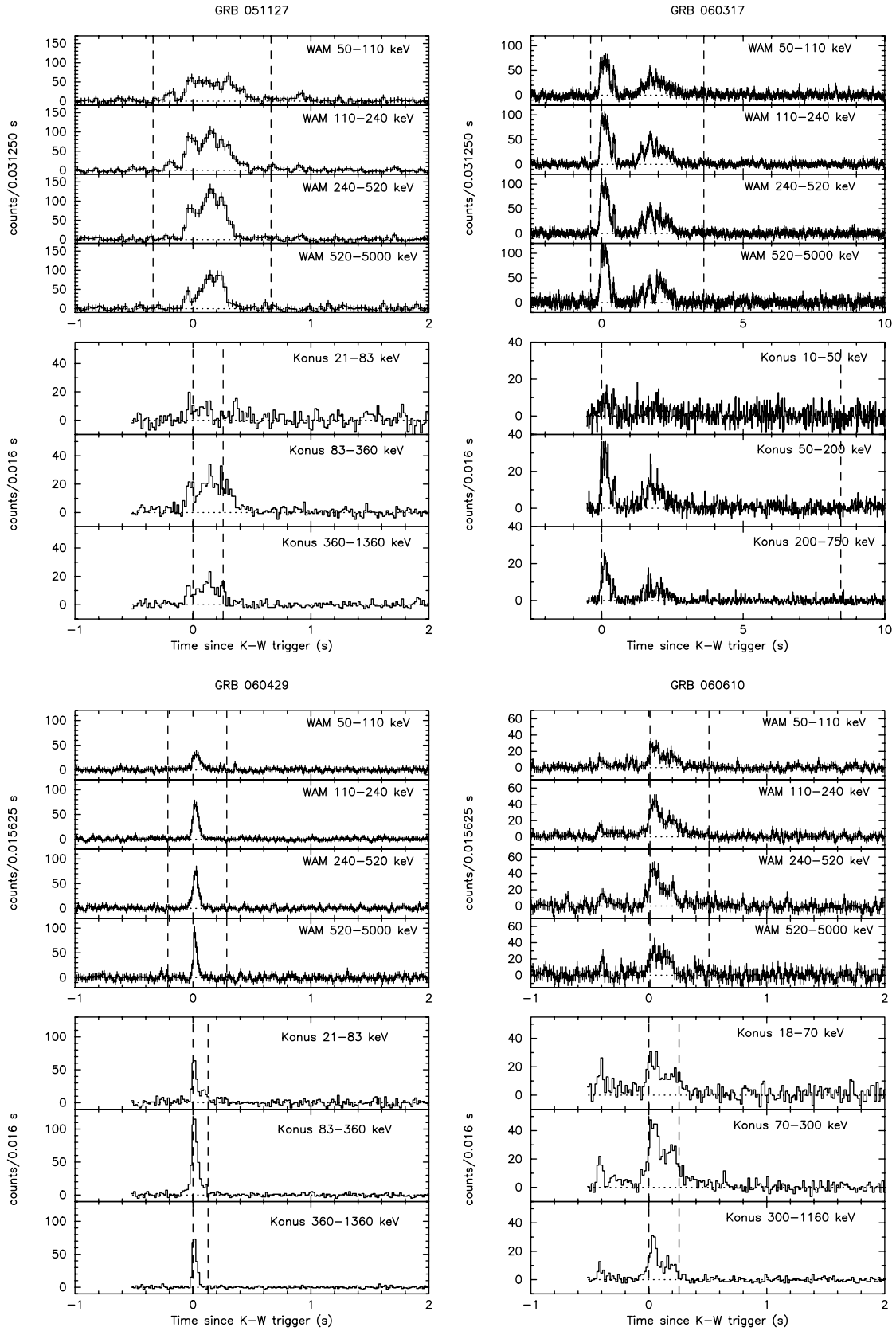
Fig. 1. Background-subtracted WAM (top) and Konus (bottom) light curves of our sample of short GRBs. The zero times of these light curves are adjusted to the Konus trigger time. The time interval for extracting the spectrum is shown by the dashed-line. Left-top panel is GRB 051127, right-top panel is GRB 060317, left-bottom panel is GRB 060429, and right-bottom panel is GRB 060610.
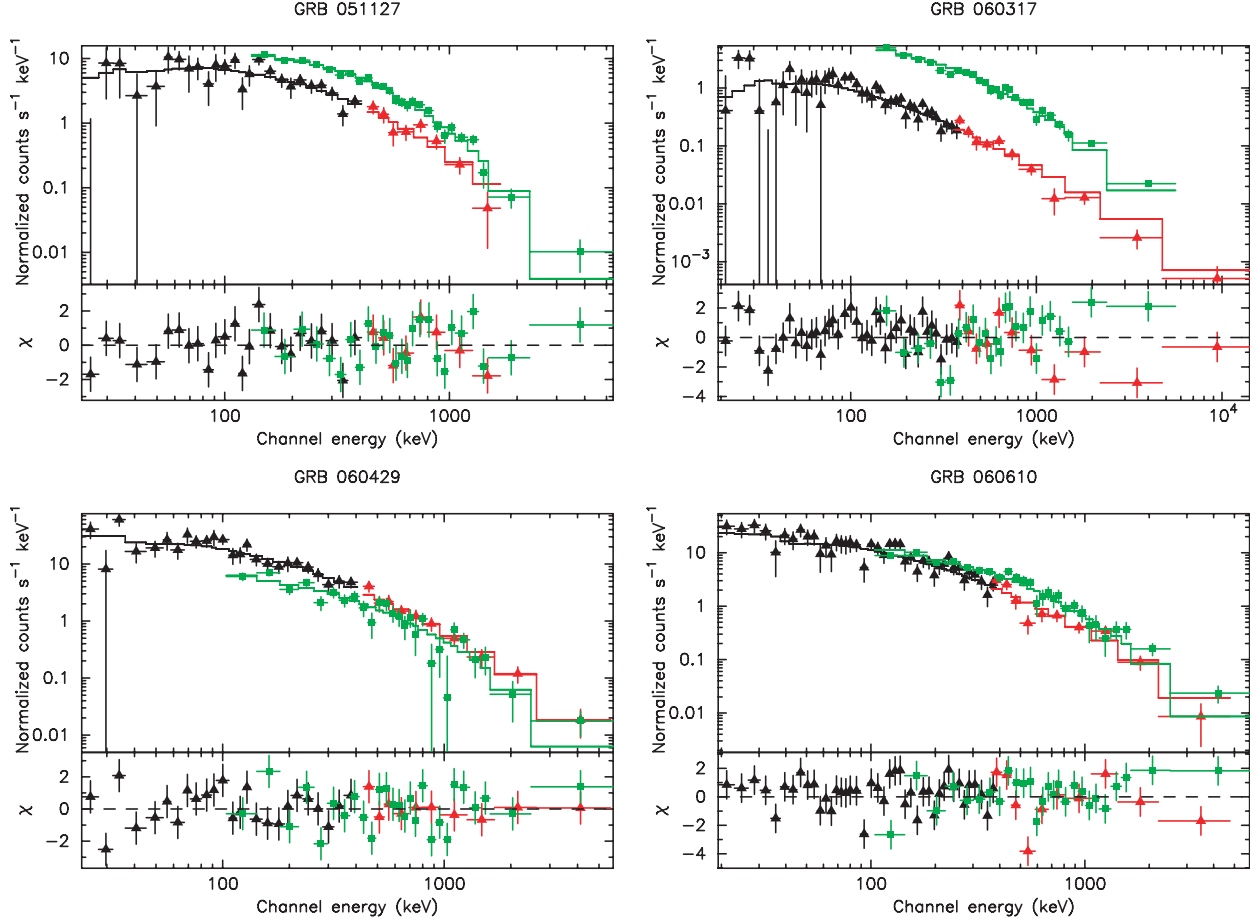
Fig. 2. Joint spectral fitting with a cut-off power law (CPL) model for the WAM (square) and the Konus (triangle) data. The solid lines represent the best-fit CPL model.

Table 4. Fluence and peak flux of our four short GRBs.

GRB	Fluence*				Peak flux[†]	
	$(10^{-6}\,\mathrm{erg\,cm^{-2}})$				$(10^{-6}\,\mathrm{erg\,s^{-1}\,cm^{-2}})$	$(\mathrm{photons\,s^{-1}\,cm^{-2}})$
	50–100 keV	100–300 keV	300–500 keV	500–1000 keV		
GRB 051127	$0.16^{+0.02}_{-0.02}$	$0.93^{+0.08}_{-0.09}$	$1.1^{+0.11}_{-0.11}$	$2.31^{+0.24}_{-0.24}$	$28^{+3.2}_{-3.2}$	$22^{+2.5}_{-2.5}$
GRB 060317	$0.72^{+0.06}_{-0.06}$	$2.60^{+0.02}_{-0.02}$	$2.38^{+0.02}_{-0.02}$	$5.47^{+0.04}_{-0.04}$	$46^{+3.8}_{-3.7}$	$41^{+3.4}_{-3.3}$
GRB 060429	$0.10^{+0.01}_{-0.01}$	$0.49^{+0.04}_{-0.04}$	$0.49^{+0.05}_{-0.05}$	$1.10^{+0.12}_{-0.12}$	$67^{+6.7}_{-5.7}$	$77^{+7.7}_{-6.6}$
GRB 060610	$0.13^{+0.01}_{-0.01}$	$0.55^{+0.04}_{-0.04}$	$0.52^{+0.05}_{-0.05}$	$1.12^{+0.11}_{-0.10}$	$33^{+2.3}_{-2.3}$	$34^{+2.3}_{-2.3}$

* The energy fluence obtained by the CPL model in the joint fitting of the WAM data.
[†] The energy and photon peak flux in 1/32 s for GRB 051127 and 060317, and in 1/64 s for GRB 060429 and 060610, respectively, obtained by the WAM 50–5000 keV data.

on duration alone, it is short enough to be placed in the short class. Since we changed the WAM time resolution from 1.0 s to 0.5 s for spectral data, and from 1/32 s to 1/64 s for light curve data on 2006 March 20, we could select the time region to be $T_0(\mathrm{WAM})$ to $T_0(\mathrm{WAM}) + 0.5$ s, and obtain a better S/N. For Konus, we selected the time interval from $T_0(\mathrm{KW})$ to $T_0(\mathrm{KW}) + 0.128$ s. The propagation delay from Suzaku to Wind is 1.530 s for this GRB, i.e., correcting for this factor,

one sees that the $T_0(\mathrm{KW}) = T_0(\mathrm{WAM}) + 0.211$ s. We can see in figure 2 that the emission extends up to 5 MeV for both WAM and Konus. We thus performed spectral fittings from 100 keV to 5 MeV for the WAM and from 20 keV to 5 MeV for Konus, respectively. These spectra are also well described by the CPL model with a high E_{peak}. The photon index is $-0.99^{+0.26}_{-0.28}$ for the WAM and $-0.76^{+0.15}_{-0.13}$ for Konus, respectively. The E_{peak} can be constrained to 1583^{+429}_{-371} keV by Konus, but the WAM
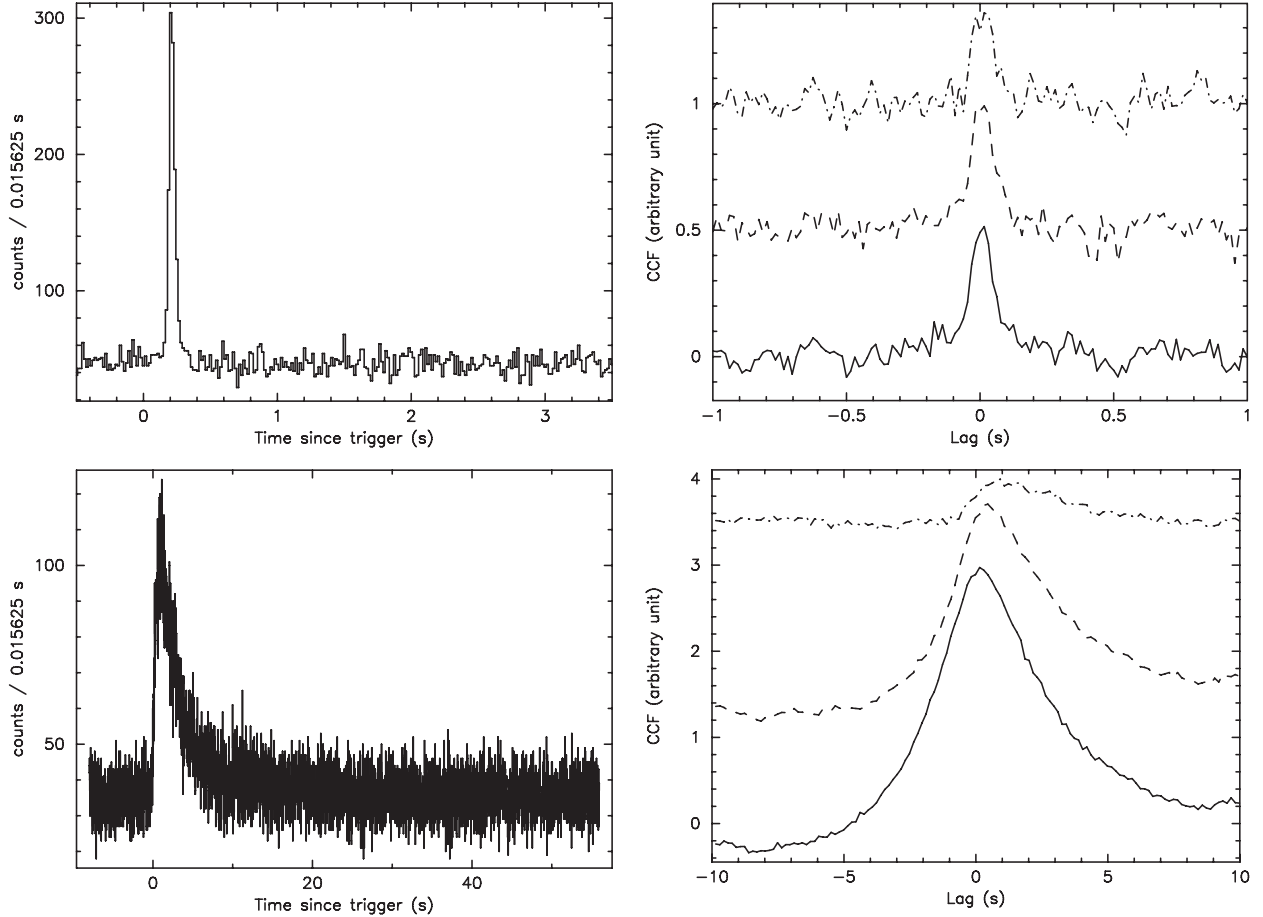
Fig. 3. Example of the light curves of the WAM data (left panels) and the CCFs (right panels) for a short GRB 060429 (top) and a long GRB 060922 (bottom). The solid line shows CCF(50–110 keV to 110–240 keV), the dashed line shows CCF(50–110 keV to 240–520 keV), and the dot-dashed line shows CCF(50–110 keV to 520–5000 keV).

data do not constrain it. The fit does not improve in the Band model. The joint fit also gives consistent results.

3.4.　GRB 060610

We can regard this GRB as short, based on the WAM burst duration of 0.79 s alone. The light curve exhibits a double-peak structure, as shown in figure 1. The time regions for spectral analysis were selected from $T_0(\text{WAM}) + 0.5$ s to $T_0(\text{WAM}) + 1.0$ s and from $T_0(\text{KW})$ to $T_0(\text{KW}) + 0.256$ s. The propagation delay between these two instruments was 1.402 s, i.e., correcting for this factor, one sees that the $T_0(\text{KW}) = T_0(\text{WAM}) + 0.490$ s. Figure 2 shows that the emission extends up to 5 MeV for both instruments. We thus performed spectral fittings from 100 keV (WAM) and from 20 keV (Konus) to 5 MeV. Both spectra are also well described by the CPL model. The WAM and Konus photon indices are $-0.90^{+0.17}_{-0.22}$ and $-0.94^{+0.12}_{-0.11}$, respectively. The E_{peak} is constrained by the WAM and Konus to 2889^{+2973}_{-1175} keV and 1536^{+500}_{-366} keV, respectively. From the joint fit, we obtained a photon index of $-0.92^{+0.09}_{-0.12}$ and an E_{peak} of 1821^{+495}_{-364} keV. There is no significant improvement of the fit with the Band model, and we can not constrain the power-law photon index, β, at high energies; we obtained an upper limit of $\beta < -2.50$.

3.5.　Spectral Lag

Figure 3 (top) shows an example of the cross correlation function (CCF) calculated for GRB 060429. The CCFs of our four short GRBs all exhibit a sharp shape structure around zero. We estimate the peak values of the CCFs using Gaussian profiles (Yi et al. 2006). The results are given in table 5. The spectral lags are all consistent with zero for all energy ranges. For a comparison, we also calculated the CCFs of three bright long WAM GRBs: 050924, 060915, and 060922. Their CCFs display broad peaks, as shown in figure 3 (bottom). Thus, we used a polynomial instead of a Gaussian profile to estimate the peak values; the results are also given in table 5. We found that these long GRBs have significant positive lags, which become larger towards the higher energy bands. We confirmed that this lag is not caused artificially, by analyzing simulated data with no spectral lag, and indeed obtained zero lag.

4.　Discussion

4.1.　Spectral Characteristics of Short GRBs

The spectra of all four GRBs are well described by a power law with an exponential cut-off (CPL), and the fits do not improve significantly when we apply the Band model. To

Table 5. Duration (T_{90}) and spectral lag (τ_{lag}) of four short GRBs and two long GRBs obtained by the WAM data.

GRB date	T_{90}* (s)	τ_{lag} (TH0,TH1)[†]	τ_{lag} (TH0,TH2)[†] (ms)	τ_{lag} (TH0,TH3)[†]
		short GRBs		
051127	0.66	17^{+18}_{-21}	13^{+14}_{-14}	7.1^{+23}_{-18}
060317	1.31	$5.1^{+5.7}_{-5.9}$	$8.4^{+5.6}_{-6.0}$	$7.3^{+8.4}_{-7.2}$
060429	0.08	$5.4^{+6.6}_{-12}$	12^{+14}_{-15}	11^{+26}_{-28}
060610	0.79	-17^{+33}_{-25}	-21^{+36}_{-50}	20^{+36}_{-45}
		long GRBs		
050924	29.09	263^{+83}_{-59}	588^{+89}_{-124}	1255^{+525}_{-266}
060915	43.16	56^{+27}_{-18}	131^{+30}_{-30}	170^{+62}_{-72}
060922	13.88	199^{+47}_{-31}	505^{+36}_{-56}	1004^{+116}_{-141}

* T_{90} duration measured in 50–5000 keV energy band of the WAM light curve.
[†] The energy bands of TH0, TH1, TH2, and TH3 correspond to 50–110 keV, 110–240 keV, 240–520 keV, and 520–5000 keV, respectively.

investigate the possibility that the spectra are better described by the Band model, we used the Band model with a typical value of the power law photon index in the high-energy portion of $\beta = -2.3$. When we performed joint fits with this model, the χ^2/d.o.f. became 66/55, 69/58, and 107/75 for GRB 051127, 060429, and 060610, respectively. For GRB 060317, there was also no improvement in the Konus spectrum with this model, whose χ^2/d.o.f. is 53/49 (see table 3). Therefore, we cannot determine whether these GRBs follow the CPL model or the Band model from our data. The power-law photon index, α, of the low-energy part of our sample is distributed around -1.0 and the mean value is -0.73. This is larger than that of the BATSE long duration GRBs of -1.05 (Ghirlanda et al. 2002). In particular for GRB 051127, there is a significantly flatter photon index of -0.41, which is larger than the synchrotron limit of $-2/3$. This distribution of α was also reported for BATSE bright, short duration GRBs (Ghirlanda et al. 2004). They showed that the spectra of their short GRB sample were also described by a CPL model. If a flat slope is a global characteristic of the prompt emission spectrum of short GRBs, the simple synchrotron emission model may no longer be applied and other emission mechanisms, such as jitter radiation (Medvedev 2000), are required.

4.2. Classification of Short GRBs

It is ambiguous in some cases to classify GRBs using the burst duration alone, because the observed long and short duration distributions overlap around 1.0–2.0 s. The dilation of the intrinsic duration of GRBs due to cosmological distance, and the dependence of duration on energy, must also be considered. Therefore, we utilize several other methods of classifying short and long GRBs below. In this section, we discuss whether the four bursts are really in the short class by examining these criteria: (1) spectral lag, (2) spectral hardness, (3) radiation energy, and (4) extended emission. So far, these criteria have been confirmed mainly based on the BATSE data. We can test these criteria in a higher energy band than BATSE by the WAM and Konus data with high statistics even in MeV energy band.
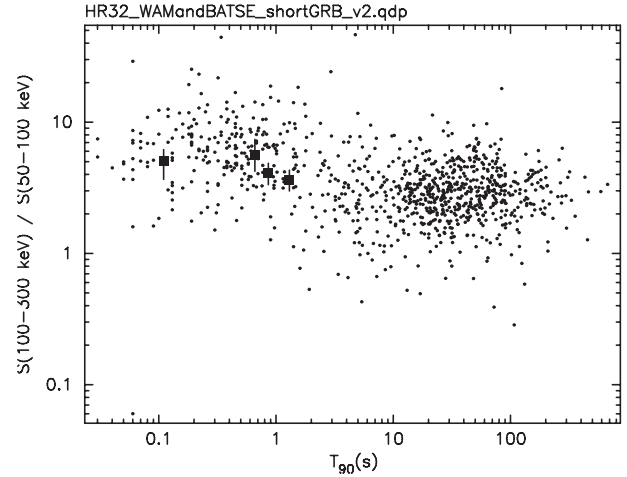
The properties of the spectral lag are reported to differ between short and long-duration GRBs. Short GRBs exhibit lags, which are consistent with zero, while long GRBs have significantly non-zero positive spectral lag (Norris et al. 2000; Norris & Bonnell 2006). We have measured the spectral lags using the WAM light curves. Figure 4 plots the relation between the duration and the spectral lag for four short GRBs, for 50–110 keV vs. 110–240 keV, 50–110 keV vs. 240–520 keV, and 50–110 keV vs. 520–5000 keV. We also plot the lags of three bright long duration WAM GRBs for comparison. We find that the spectral lag of all four short GRBs is consistent with zero in approximately the same energy bands as BATSE (50–110 keV vs. 110–240 keV or 50–110 keV vs. 240–520 keV), while non-zero lag, evolving with T_{90}, is seen for the three long GRBs. Therefore, the WAM data confirm the difference in the spectral lag obtained with BATSE. In addition, figure 4 demonstrates the WAM capabilities in the high-energy band: lag evolution is seen above 520 keV for long GRBs.

The hardness ratio of short GRBs is reported to be slightly harder than that of long GRBs from BATSE results (Cline et al. 1999; Paciesas et al. 1999). Although the boundary between short and long GRBs in the duration–hardness plane is ambiguous, we nevertheless consider this difference as a possible criterion. Therefore, we obtained the spectral hardness of our sample of short GRBs, based on the best-fit spectral model. We derived the hardness ratio using the 50–100 and 100–300 keV fluence, which is same energy range as BATSE. We plot them against the T_{90} duration in figure 5, together with the BATSE results (Paciesas et al. 1999). The hardness ratios of our short GRBs are distributed from 3.61 to 5.64 with an average value of 4.61, and all have greater hardness ratios than the average value of the BATSE long ($T_{90} > 2.0$) GRBs (3.27). Therefore, all four are consistent with a short classification. However, these short GRBs do not show a clear separation from the long GRBs, as in the BATSE samples in figure 5. Although all our short GRBs have an E_{peak} around 1 MeV, none of them exceeds a hardness ratio of 8, whereas half of the BATSE short GRBs do. This is because the
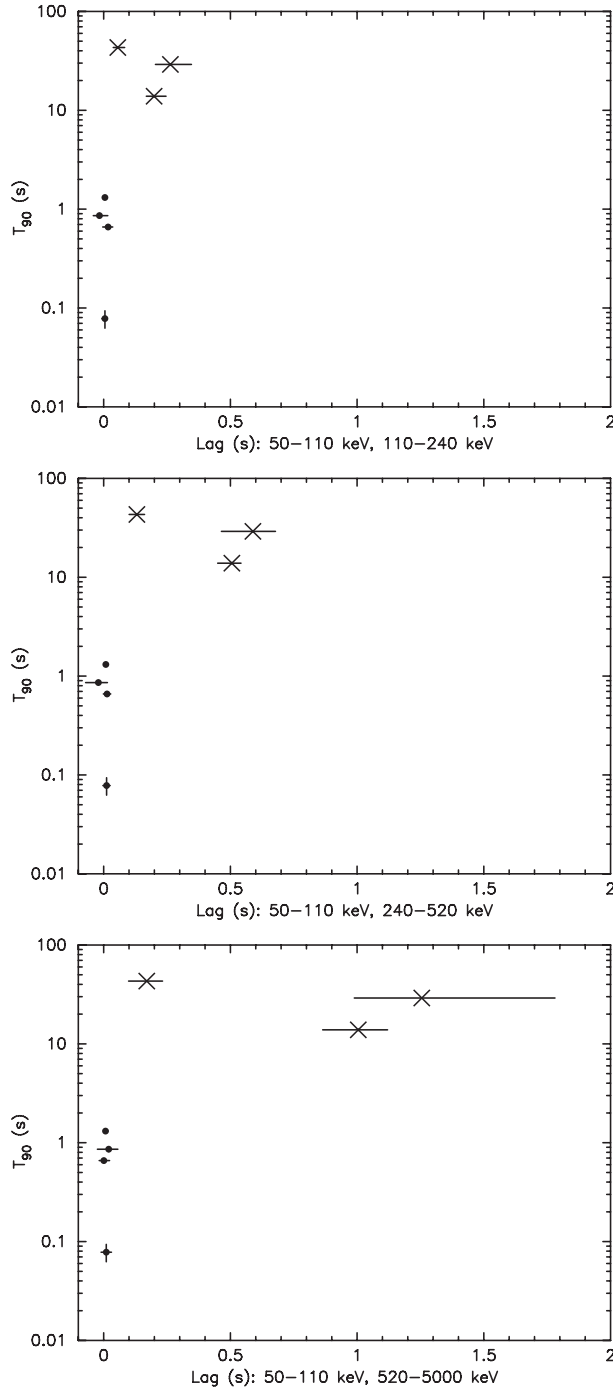
Fig. 4. Relation of the T_{90} duration and the spectral lag. From top to bottom, the lag of 50–110 keV to 110–240 keV, 50–110 keV to 240–520 keV, and 50–110 keV to 520–5000 keV are shown. The filled circles are for the four short GRBs of this paper and the crosses are for long GRBs.

Fig. 5. Relation between the duration (T_{90}) and the hardness ratio of 100–300 keV to 50–100 keV. The dots show BATSE results. The results of our four short GRBs are shown as filled squares.
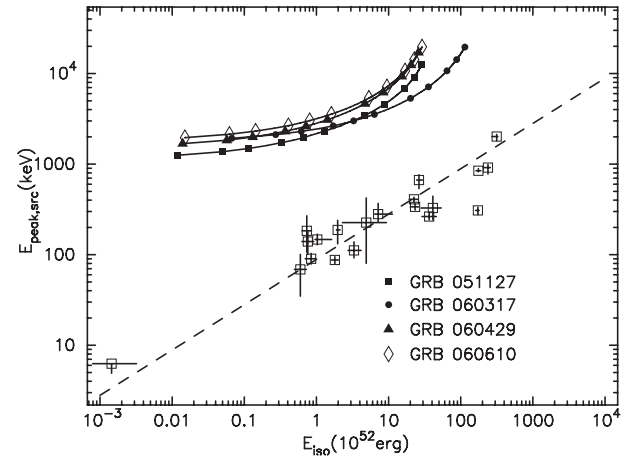
Fig. 6. Relation between $E_{\rm peak}$ and $E_{\rm iso}$ for our four short GRBs (filled square, GRB 051127; filled circle, GRB 060317; filled triangle, GRB 060429; and open diamond, GRB 060610). The trajectories were calculated by assuming redshifts from 0.1 to 10.0. The data points along the trajectories correspond to $z = 0.1, 0.2, 0.3, 0.5, 0.7, 1.0, 2.0,$ 3.0, 5.0, 7.0, and 10.0, respectively. Open squares are the HETE-2 and Beppo SAX results (Sakamoto et al. 2005a). The dashed-line represents the Amati relation $E_{\rm peak,src} \propto E_{\rm iso}^{0.5}$ for long GRBs.

hardness ratio depends on the low-energy photon index rather than $E_{\rm peak}$ (Ghirlanda et al. 2004; Sakamoto et al. 2006). The short GRB which has the highest hardness ratio in our sample is GRB 051127, with $5.64^{+1.75}_{-1.42}$. GRB 051127 also has the hardest photon index, -0.44, but its $E_{\rm peak}$ is one of the lowest in our sample. As mentioned in Sakamoto et al. (2006), the

low-energy photon index has to be flatter than 0 to reproduce a hardness ratio greater than 8, which is seen in the BATSE "very hard" short GRBs. Based on our broad band spectroscopy of bright, high $E_{\rm peak}$ short GRBs, none has a hardness ratio similar to the BATSE "very hard" short GRBs.

For long GRBs, a correlation between the peak energy and the isotropic equivalent radiation energy in the source frame has been reported: the Amati relation (Amati et al. 2002). However, short GRBs whose redshifts are known have lower isotropic energy than long GRBs and do not satisfy this relation (Amati 2006). We calculated the isotropic energy, $E_{\rm iso}$, of our four short GRBs from 1.0 to 10000 keV in the source frame, assuming redshifts from 0.1 to 10.0. We used

cosmological parameters $(H_0, \Omega_\Lambda, \Omega_m) = (65, 0.7, 0.3)$. We included the effects of redshift on the energy spectra and E_{peak} of these bursts. Figure 6 shows the results of the calculation in the E_p-E_{iso} plane together with the HETE-2 and BeppoSAX results (Sakamoto et al. 2005a). We could not find any redshift that satisfies the Amati relation. All of the bursts in our sample exhibit a lower isotropic radiation energy by more than one order of magnitude when compared with long bursts of the same peak energy. This is consistent with previous results.

Long, soft emission humps a few tens of seconds after the short main spike were reported for several short GRBs (Norris & Bonnell 2006), particularly GRB 050709 (Villasenor et al. 2005) and 050724 (Barthelmy et al. 2005), which have measurements of the redshift and detections of the host galaxy. Thus the existence of the soft emission hump is considered to be one of the criteria to classify short GRBs. We searched for long soft humps in the time histories of our four short GRBs, but did not detect them. To do this, we calculated the upper limits to the peak soft photon flux at the 3σ level for the WAM and Konus. In this calculation, we assumed that the spectrum of the soft emission was a simple power law with a photon index -2.0. We found 3σ upper limits to the 2.0 to 25 keV peak flux of 4.47, 6.63, 9.21, and 7.54 photons s^{-1} cm^{-2}, for GRB 051127, 060317, 060429, and 060610, respectively, using both the WAM and Konus. All of these values exceed 2.72 (±0.47), which was obtained for GRB 050709 (Villasenor et al. 2005). Therefore, the non-detection of the soft emission for these bursts adds no constraint: the extended emission could be too soft to be detected by the WAM and Konus.

5. Conclusions

We performed a joint analysis of four bright, hard-spectrum, short-duration GRBs, localized by the IPN, with the Suzaku-WAM and Konus-Wind, in order to investigate the spectral properties of short GRBs into the MeV energy band. From the spectral analysis, we found that these bursts have a high E_{peak} around 1 MeV; the spectral parameters can be constrained tightly by joint fitting. However, we could not determine whether these spectra follow the CPL model or the Band model, because there is no significant improvement between these models. The power-law photon index is slightly flatter than that of long BATSE GRBs. In particular, GRB 051127 has a very flat spectrum with a photon index $\alpha = -0.41$, that is larger than the synchrotron limit of $-2/3$.

We also examined several other spectral and temporal properties to confirm that the bursts belong to the short class. Most properties, such as the spectral lag, the spectral hardness, and the isotropic radiation energy, indicated that the four bursts were indeed in this class. In addition, a broad-band spectral analysis with the WAM and Konus revealed some interesting properties of short GRBs: (1) There is no evidence for very hard GRBs that have the large hardness ratios seen in BATSE short GRBs. (2) The spectral lag of our short GRBs does not show any clear evolution, even in the MeV energy region, unlike that of long hard GRBs. Although our short GRB sample is still limited, these results might suggest one possibility, that the hardness ratios of the short GRBs are not so different from those of long GRBs, and also that the spectral lag at high energies can be a strong criterion for classifying short and long GRBs.

References

Arnaud, K. 1996, in ASP Conf. Ser. 101, Astronomical Data Analysis Software and Systems V, ed. G. H. Jacoby & J. Barnes (San Francisco: ASP), 17

Amati, L. 2006, MNRAS, 372, 233

Amati, L., et al. 2002, A&A, 390, 81

Aptekar, R. L., et al. 1995, Space Sci. Rev., 71, 265

Band, D. L. 1997, ApJ, 486, 928

Band, D., et al. 1993, ApJ, 413, 281

Barthelmy, S. D., et al. 2005, Nature, 438, 994

Cline, B. D., Matthey, C., & Otwinowski, S. 1999, ApJ, 527, 827

Cummings, J., et al. 2006, GCN Circ., 5005

Dezalay, J.-P., Barat, C., Talon, R., Sunyaev, R., Terekhov, O., & Kuznetsov, A. 1992, in AIP Conf. Proc. 265, Gamma-Ray Bursts, ed. W. S. Paciesas & G. J. Fishman (New York: AIP), 304

Donaghy, T. Q., et al. 2006, astro-ph 0605570

Fox, D. B., et al. 2005, Nature, 437, 845

Fox, D. B., & Moon, D. S. 2004, GCN Circ., 2734

Frontera, F., et al. 2000, ApJS, 127, 59

Gehrels, N., et al. 2004, ApJ, 611, 1005

Gehrels, N., et al. 2006, Nature, 444, 1044

Ghirlanda, G., Celotti, A., & Ghisellini, G. 2002, A&A, 393, 409

Ghirlanda, G., Ghisellini, G., & Celotti, A. 2004, A&A, 422, L55

Golenetskii, S., et al. 2006a, GCN Circ., 4856

Golenetskii, S., et al. 2006b, GCN Circ., 5067

Hjorth, J., et al. 2003, Nature, 423, 847

Hjorth, J., et al. 2005 Nature, 437, 859

Hullinger, D., et al. 2005, GCN Circ., 4400

Hurley, K. 1992, in AIP Conf. Proc. 265, Gamma-Ray Bursts, 1991 ed. W. Paciesas & G. Fishman (New York: AIP), 3

Hurley, K., et al. 2006a, ApJS, 164, 124

Hurley, K., et al. 2006b, GCN Circ., 5039

Kaneko, Y., Preece, R. D., Briggs, M. S., Paciesas, W. S., Meegan, C. A., & Band, D. L. 2006, ApJS, 166, 298

Katz, J. I., & Canel, L. M. 1996, ApJ, 471, 915

Kokubun, M., et al. 2007, PASJ, 59, S53

Kouveliotou, C., Meegan, C. A., Fishman, G. J., Bhat, N. P., Briggs, M. S., Koshut, T. M., Spaciesas, W. S., & Pendleton, G. N. 1993, ApJ, 413, L101

Ling, J. C., et al. 2000, ApJ, 127, 79

Link, B., Epstein, R. I., & Priedhorsky, W. C. 1993, ApJ, 408, L81

Mazets, E. P., et al. 1981, Ap&SS, 80, 119

Medvedev, M. V. 2000, ApJ, 540, 704

Mitsuda, K., et al. 2007, PASJ, 59, S1

Norris, J. P. 2002, ApJ, 579, 386

Norris, J. P., & Bonnell, J. T. 2006, ApJ, 643, 266

Norris, J. P., Cline, T. L., Desai, U. D., & Teegarden, B. J. 1984, Nature, 308, 434

Norris, J. P., Nemiroff, R. J., Bonnell, J. T., Scargle, J. D., Kouveliotou, C., Paciesas, W. S., Meegan, C. A., & Fishman, G. J. 1996, ApJ, 459, 393

Norris, J. P., Scargle, J. D., & Bonnell, J. T. 2000, BAAS, 32, 1244

Ohno, M., et al. 2005, IEEE Trans. Nucl. Sci., 52, 2758

Paciesas, W. S., et al. 1999, ApJ, 122, 465

Paciesas, W. S., Preece, R. D., Briggs, M. S., & Mallozzi, R. S. 2001, in Gamma Ray Bursts in the Afterglow Era, ed. E. Costa, F. Frontera, & J. Hjarth (Berlin: Springer), 13

Rau, A., von Kienlin, A., Hurley, K., & Lichti, G. 2005, A&A 438, 1175

Ricker, G. R., et al. 2003, in AIP Conf. Proc. 662, Gamma-Ray Burst and Afterglow Astronomy 2001, ed. G. R. Ricker & R. K. Vanderspek (New York: AIP), 3

Ruffert, M., & Janka, H.-T. 1999, A&A, 344, 573

Sakamoto, T., et al. 2005a, ApJ, 629, 311

Sakamoto, T., et al. 2005b, GCN Circ., 4403

Sakamoto, T., et al. 2006, in AIP Conf. Proc. 836, Gamma-Ray Bursts in the Swift Era 2005, ed. S. S. Holt, N. Gehrels, & J. A. Nousek (New York: AIP), 43

Takahashi, T., et al. 2007, PASJ, 59, S35

Villasenor, J. S., et al. 2005, Nature, 437, 855

Wiersema, K., Starling, R. L. C., Rol, E., Vreeswijk, P., & Wijers, R. A. M. J. 2004, GCN Circ., 2800

Yamaoka, K., et al. 2005, IEEE Trans. Nucl. Sci., 52, 2765

Yamaoka, K., et al. 2006, Proc. SPIE, 6266, 153

Yi, T., Liang, E., Qin, Y., & Lu, R. 2006, MNRAS, 367, 1751